Research Paper

Redox homeostasis and cell cycle activation mediate beta-cell mass expansion in aged, diabetes-prone mice under metabolic stress conditions: Role of thioredoxin-interacting protein (TXNIP)

Richard Kehm [a,c], Markus Jähnert [b,c], Stefanie Deubel [a], Tanina Flore [a], Jeannette König [a], Tobias Jung [a,f], Mandy Stadion [b,c], Wenke Jonas [b,c], Annette Schürmann [b,c,f], Tilman Grune [a,c,d,e,f], Annika Höhn [a,c,*]

[a] Department of Molecular Toxicology, German Institute of Human Nutrition Potsdam-Rehbruecke (DIfE), 14558, Nuthetal, Germany
[b] Department of Experimental Diabetology, German Institute of Human Nutrition Potsdam-Rehbruecke (DIfE), 14558, Nuthetal, Germany
[c] German Center for Diabetes Research (DZD), 85764, Muenchen-Neuherberg, Germany
[d] NutriAct-Competence Cluster Nutrition Research Berlin-Potsdam, 14458, Nuthetal, Germany
[e] German Center for Cardiovascular Research (DZHK), 10117, Berlin, Germany
[f] University of Potsdam, Institute of Nutritional Science, 14558, Nuthetal, Germany

ARTICLE INFO

ABSTRACT

Overnutrition contributes to insulin resistance, obesity and metabolic stress, initiating a loss of functional beta-cells and diabetes development. Whether these damaging effects are amplified in advanced age is barely investigated. Therefore, New Zealand Obese (NZO) mice, a well-established model for the investigation of human obesity-associated type 2 diabetes, were fed a metabolically challenging diet with a high-fat, carbohydrate restricted period followed by a carbohydrate intervention in young as well as advanced age. Interestingly, while young NZO mice developed massive hyperglycemia in response to carbohydrate feeding, leading to beta-cell dysfunction and cell death, aged counterparts compensated the increased insulin demand by persistent beta-cell function and beta-cell mass expansion. Beta-cell loss in young NZO islets was linked to increased expression of thioredoxin-interacting protein (TXNIP), presumably initiating an apoptosis-signaling cascade via caspase-3 activation. In contrast, islets of aged NZOs exhibited a sustained redox balance without changes in TXNIP expression, associated with higher proliferative potential by cell cycle activation. These findings support the relevance of a maintained proliferative potential and redox homeostasis for preserving islet functionality under metabolic stress, with the peculiarity that this adaptive response emerged with advanced age in diabetes-prone NZO mice.

1. Introduction

Pancreatic islets, especially their insulin-releasing beta-cells are crucial for the regulation of glucose homeostasis in response to nutrient supply. An impairment of beta-cell functionality and integrity has harmful effects on the whole-body energy metabolism and is fundamental for type 2 diabetes pathogenesis [1,2]. In this context, overnutrition by high-caloric diets, composed of carbohydrates and fats, initiate peripheral insulin resistance, obesity and systemic inflammation, followed by metabolic stress conditions, known as glucolipotoxicity. During certain physiological states, such as obesity or pregnancy, pancreatic islets are able to increase the secretory potential and expand their beta-cell mass, primarily by compensatory proliferation to appropriately adjust on insulin requirements [3,4]. On a molecular level, different intracellular signaling pathways have been elucidated mainly in rodents, inducing beta-cell proliferation by a network of several cell cycle activators, such as cyclins and cyclin-dependent kinases (CDK) [5]. However, persistent and repeated elevated circulating glucose and fatty acids have been linked to a

Nomenclature

ASK1   Apoptosis signal-regulating kinase 1
CDK   Cyclin-dependent kinases
-CH   Carbohydrate-free, high-fat diet
+CH   Carbohydrate-rich diet
GO   Gene ontology
IPA   Ingenuity pathway analysis
NZO   New Zealand Obese
PDX1   Pancreatic and duodenal homeobox 1
TXN1/2 Thioredoxin 1/2
TXNIP   Thioredoxin-interacting protein

gradual decline in the proliferative as well as secretory potential of beta-cells and promote apoptotic cell death [6–9]. High blood glucose levels are also linked to the induction of oxidative stress in beta-cells due to the endogenous formation of reactive oxygen species (ROS). This becomes apparent by the naturally low defense potential of beta-cells based on their low expression of essential anti-oxidative enzymes, such as superoxide-dismutase or catalase [10–12]. In this context, several previous investigations demonstrate that thioredoxin-interacting protein (TXNIP) serves as a critical mediator of hyperglycemia-induced beta-cell failure and death via different mechanisms. TXNIP inhibits the thioredoxin (TXN) pathway by binding to the reduced form of TXN1, downregulates essential transcription factors for insulin production and triggers the mitochondrial death pathway by binding to mitochondrial TXN2 and activation of caspase-3 [13–17]. Thus, TXNIP regulates beta-cell redox homeostasis by inhibiting their anti-oxidative potential, in turn, leading to higher susceptibility towards oxidative damage and apoptosis [14,18]. Besides dietary factors, aging and related alterations have been shown to influence beta-cell characteristics. Recently, we demonstrated that pancreatic islets of normoglycemic wild-type mice progressively lose their proliferative and regenerative potential, associated with the induction of cellular senescence, known to induce an irreversible cell cycle arrest [19]. Furthermore, different well-known hallmarks of aging, such as mitochondrial dysfunction, elevated oxidative stress and inflammation, all linked to a dysregulated redox balance, affect beta-cells by impairing their secretory function and survival. In combination, this might lead to a decline of insulin action in peripheral tissues, beta-cell functional exhaustion and death [20–22]. To what extent aging under metabolic stress conditions affects beta-cell characteristics and functionality remains widely unknown. Therefore, young and aged diabetes-prone New Zealand Obese (NZO) mice were used to investigate the impact of advanced age in combination with diet-induced metabolic stress on beta-cell functionality as well as structural integrity.

2. Material and methods

2.1. Animal procedures, diets and study design

Male NZO mice (NZO/HIBomDife mice, German Institute of Human Nutrition, Potsdam-Rehbruecke, Germany) were housed in open cages of 4–5 animals at a controlled environment (20 ± 2°C, 12/12 h light/dark cycle) with *ad libitum* access to diets and water. As shown in Fig. 1A, after weaning and feeding a control diet (V1534-300, Ssniff, Soest, Germany), seven-weeks old mice were randomly assigned into young and aged groups. Both groups received a carbohydrate-free, high-fat diet [-CH, 32.1% (wt/wt) protein and 30.6% (wt/wt) fat, #C105789, Altromin, Lage, Germany] for 11 weeks (young) or 32 weeks (aged). Subgroups were fed with a carbohydrate-rich diet [+CH, 20% (wt/wt) protein, 28% (wt/wt) fat and 40% (wt/wt) carbohydrates] for a maximum of 21 days (for detailed diet compositions, see Ref. [23]). A

further extension of the metabolic challenge was not permitted for animal welfare reasons. Mice age at the end of the study (42 weeks) corresponds to middle-aged [24]. However, due to severe obesity, especially in aged groups in response to the metabolic challenge, it might be assumed that the dietary regimen resulted in accelerated aging of our cohorts [25,26]. After sacrificing by acute isoflurane exposure, blood samples were taken and pancreatic tissue samples were either fixed in 4% paraformaldehyde for 24 h with subsequent paraffin embedding or shock-frozen in liquid nitrogen. Furthermore, endocrine islets were isolated by collagenase digestion, as described below. Mice were kept in agreement with the NIH guidelines for the care and use of laboratory animals. All experiments were verified and approved by the animal welfare committee of the DIfE and the ethics committee of the State Office Environment, Health, and Consumer Protection (Germany, Brandenburg, approval number: V3-2347-21-2015).

2.2. Assessment of glucose utilization

Body weight and blood glucose measurements were monitored in a 2-weeks interval and immediately before sacrificing the mice at indicated time points by using a CONTOUR® XT glucometer (Bayer, Leverkusen, Germany). For oral glucose tolerance test, blood samples of fasted mice (16 h overnight) were taken from the tail vein and blood glucose was measured at 0, 15, 30, 60 and 120 min after oral administration with 20% glucose solution (Braun, Melsungen, Germany). Energy expenditure in young and aged animals before and after 21 days of the carbohydrate intervention was determined by using indirect calorimetry (PhenoMaster, TSE Systems, Bad Homburg, Germany). Animals were adapted to respiratory cages for 24 h followed by a 72 h measurement in a controlled environment at 22°C with free access to food and water. Mean values over 48 h starting after 1 day of the measurement were included in the calculation. Energy expenditure was normalized to body weight and expressed in kcal/g/h.

2.3. Determination of plasma insulin and pancreatic insulin content

The concentration of plasma insulin was measured by performing a Mouse Ultrasensitive Insulin ELISA (ALPCO, Salem, USA), according to supplier's instructions. The entire pancreatic insulin content was determined in freshly isolated pancreas. Placed in ice-cold acidic ethanol, samples were homogenized with a ball mill for 5 min at maximum speed and incubated overnight at 4°C. Pancreatic lysates were centrifuged for 10 min (16.000 rpm, 4°C) and insulin was detected in the supernatant fraction, again by Mouse Ultrasensitive Insulin ELISA (ALPCO, Salem, USA).

2.4. Isolation of pancreatic islet and microarray-based transcriptomics

The isolation of islets from NZO mice before and after 2 as well as 21 days of +CH feeding was performed as previously described with slight modifications [27]. Due to the small number of isolated NZO islets, some samples had to be pooled. After perfusion by injection of 3 ml Collagenase Type IV from *Clostridium histolyticum* (Sigma-Aldrich, Taufkirchen, Germany) diluted in Hank's buffered salt solution (plus 25 mM HEPES, 0,5% BSA) into the common bile duct, the pancreas was digested in 2 ml of collagenase for 12 min at 37°C. After mechanical tissue disruption by using a 18G needle, samples were washed and sedimented three times in Hank's buffered salt solution and islets were separated from exocrine tissue by manual selection in RPMI1640 (plus 10% FCS, 2% L-Glutamine, 1% penicillin/streptomycin).

Total RNA isolation and microarray-XS-based transcriptome analysis of islets on day 0 and after 2 days of the diet change was performed by Oak-Labs GmbH (Berlin, Germany). Briefly, RNA extracts underwent a quality control with the Agilent 2100 Bioanalyzer (Agilent Technologies, Waldbronn, Germany) and samples with a minimal RNA integrity number of 8.0 (RIN) were included in microarray analysis. For the

generation of fluorescent cRNA, the low Input QuickAmp Labeling Kit (Agilent Technologies, Waldbronn, Germany) was used. Fluorescent signals were detected by a SurePrint G3 Mouse GE 8 × 60 k chip (Agilent Technologies, Waldbronn, Germany). Microarray data were analyzed with Software R (version 3.4.1) [28]. Web-based GOrilla tool was used to identify biological processes influenced by the entirety of differentially expressed transcripts (http://cbl-gorilla.cs.technion.ac.il/, 03/17/2020). The list of differentially expressed transcripts was ranked by log2 fold change (log2FC) to detect enriched GO terms of young and aged NZO mice before and after 2 days of the diet switch [29]. Top 10 ranking and pathway analysis of top 100 up- and downregulated transcripts were generated by using Qiagen IPA (content version: 44691306, QIAGEN Bioinformatics, Hilden, Germany). After quantile normalization, fold change and p-values were calculated. P-values have been calculated using two-tailed Students t-test with Welch correction, utilizing the "stats" R-package version 3.1.1. Different expressions between groups were testified when a threshold of $p < 0.05$ and a log2FC of $|0.7|$ were reached. The accession ID for raw data of murine islet microarray analysis is GEO: GSE150281.

2.5. Glucose-stimulated insulin secretion in primary mouse islets

Immediately after isolation and 1 h recovery in RPMI1640 (containing 10% FCS, 2% L-Glutamine, 1% penicillin/streptomycin) at 37°C, 45 hand-picked primary islets per sample were used to determine the insulin secretion. Islets were recovered in Krebs-Ringer solution (plus 0.2% BSA, pH 7.4) under low glucose conditions (2.8 mmol/l) for 1 h. Subsequent to the islet transfer into perifusion chambers, glucose-stimulated insulin secretion was performed following a sequence of low glucose conditions (2.8 mmol/l) for 18 min, high glucose conditions (20.0 mmol/l) for 35 min, low glucose conditions for 30 min and finally potassium chloride (40 mmol/l) for 20 min with a continuous flow of 0.5 ml/min. Insulin secretion was measured in intervals of 2–4 min. Levels of insulin were evaluated by performing a Mouse Ultrasensitive Insulin ELISA (ALPCO, Salem, USA) normalized to DNA content determined with the Quanti-iT PicoGreen dsDNA Assay Kit (Invitrogen, Carlsbad, USA).

2.6. Immunostaining and TUNEL assay in pancreatic tissue sections

For immunohistochemical and immunofluorescent analysis, longitudinal, serial sections (2 μm) of young and aged mice before and after 2 as well as 21 days of the +CH intervention were processed as previously described [19]. Pancreatic tissue slices were incubated with primary antibodies against rabbit Ki67 (1:1000, Abcam, Cambridge, UK) and mouse caspase-3 (1:100, Life Technologies, Darmstadt, Germany) for 1 h at room temperature. To determine beta-cell mass and islet number, sections were incubated with rabbit insulin antibody (1:10.000, Abcam, Cambridge, UK), visualized by using DAKO EnVision™+ System, HRP kit (Agilent, Waldbronn, Germany) and counterstained with hematoxylin (Sigma-Aldrich, Taufkirchen, Germany). Digital images of entire slides were taken with MIRAXMIDI Scanner (Zeiss, Jena. Germany). Images of insulin, Ki67 and caspase-3 stainings were quantified by using Zeiss ZEN2.3 imaging software (Zeiss, Jena, Germany). Beta-cell mass was determined by multiplying total insulin$^+$-area with pancreatic area divided by pancreas weight. Islet number per slide was counted, manually. For double immunofluorescent labeling, rabbit pancreatic and duodenal homeobox 1 (PDX1, 1:200, Merck Millipore, Darmstadt, Germany) and mouse insulin (1:1.000, Cell Signaling, Cambridge, United Kingdom) antibodies were used. For multicolor staining, tissue slices were incubated overnight at 4°C with rabbit insulin antibody (1:1000, Abcam, Cambridge, United Kingdom). After washing and a second blocking step, this was followed by 1 h incubation with primary antibodies against mouse glucagon (1:200, ab10988, Abcam, Cambridge, United Kingdom) and rat somatostatin (1:75, ab30788, Abcam, Cambridge, United Kingdom). Detection of primary antibodies was

achieved with cross-adsorbed secondary antibodies conjugated to AlexaFluor 488, 546 and 633 (1:200, Invitrogen, Darmstadt, Germany). Nuclei were visualized by embedding in FluorCare, including DAPI (Carl Roth, Karlsruhe, Germany). Apoptotic cells in pancreatic tissue sections were detected via TUNEL assay - TdT *In Situ* Apoptosis Detection Kit Fluorescein (R&D Systems, Minneapolis; USA), according to supplier's instructions. Imaging was performed by using Olympus IX53 (Olympus, Hamburg, Germany) or Zeiss LSM 780 confocal microscopes (Zeiss, Jena, Germany). Immunofluorescent images were evaluated via automated detection and quantification with an in-house programmed macro for ImageJ software package (Version 1,52 h, NIH, USA) [30].

2.7. Real-time PCR analysis

The mRNA extraction from 70 to 100 pancreatic islets was performed by using Dynabeads™ mRNA Purification Kit (Thermo Fisher Scientific, Darmstadt, Germany), following manufacturer's guidelines. Due to small amounts of available material, supernatants of islet lysates obtained during the mRNA isolation step were preserved for Western blot analysis. Subsequent to extraction, mRNA samples were reverse transcribed by SensiFAST cDNA Synthesis Kit (Bioline, London, UK) and diluted 1:10 in water, followed by RT-PCR reactions with the DreamTaq-Hot Start-DNA Polymerase (Thermo Fisher Scientific, Darmstadt, Germany) and SYBR Green (Invitrogen, Carlsbad, USA). Standard curves of diluted PCR products were monitored in parallel and used for quantification. Murine primers obtained from Sigma-Aldrich (Taufkirchen, Germany) and designed with the Primer-Blast tool of NCBI, are listed in Supplementary Table 1. Since most tested housekeeping genes (*Hrpt*, *Beta-actin*, *Gapdh* or *Tbp*) were markedly regulated by the +CH intervention, target gene expression was normalized only to *Rpl13a*.

2.8. Western immunoblot analysis

As mentioned above, islet supernatants from mRNA isolation were used for immunoblotting. Protein concentrations were determined with Lowry assay (Bio-Rad Laboratories, Munich, Germany), followed by acetone precipitation overnight at -20°C. Afterwards, samples were centrifuged for 10 min (14.000 rpm, 4°C), pellets were transferred in loading buffer and incubated for 5 min at 95°C. Subsequently, immunoblot analysis was performed by using a 15% polyacrylamide gel (20 slot chambers) loaded with 7 μg of sample. After gel electrophoresis, proteins were transferred to 4.5 μm nitrocellulose membrane via semidry blotting for 30 min. Membranes were then blocked in Odyssey© blocking buffer (LI-COR Biosciences, Lincoln, USA) for 1 h at room temperature and incubated with primary antibodies against rabbit TXNIP (1:1000, Thermo Fisher Scientific, Darmstadt, Germany) and mouse GAPDH (1:20.000, Abcam, Cambridge, UK) overnight at 4°C. This was followed by washing steps and secondary antibody incubation with mouse and rabbit fluorescent-conjugated secondary antibodies from LI-COR Biosciences (Lincol, USA). Signals were detected with an Odyssey® Infrared Imaging System (LI-COR Biosciences, Lincoln, USA).

2.9. Statistical analysis

Graph Pad Prism version 7.04 (San Diego, USA) was used for the generation of all graphs, heatmaps and statistical analysis. Data are represented as mean values ± SD. For group comparison, two-tailed Students t-test with Welch correction, one-way ANOVA with Tukey's multiple comparison test or two-way ANOVA with Sidak's multiple comparison test were performed (statistical parameters and tests are included in figure legends). Outlier tests were carried out when n > 4. Values of $p < 0.05$ were considered statistically significant, represented as letters.

3. Results

3.1. Different effects of the carbohydrate intervention on glucose homeostasis and insulin secretion in young and aged NZO mice

NZO mice are a polygenic model for obesity and type 2 diabetes, developing metabolic stress-induced beta-cell failure under a specific high-caloric dietary regimen. This is composed of an initial carbohydrate-free, high-fat diet (-CH), triggering insulin resistance and obesity, followed by a carbohydrate-rich diet (+CH) that finally leads to hyperglycemia, beta-cell dysfunction and apoptosis [31–34]. By extending the metabolic challenge, the impact of an advanced age on pancreatic beta-cells under metabolic stress conditions was examined (study design illustrated in Fig. 1A).

Even before the diet switch, young and aged NZO mice exhibit body weight gain, reinforced by prolonged –CH feeding in aged animals (Fig. 1B). In response to the intervention with +CH, circulating glucose concentrations of both young and aged NZOs increased continuously. However, aged NZO mice showed lower blood glucose levels after 2 and 21 days of the +CH challenge compared to young animals (Fig. 1C). Following the 21-day intervention, some of the aged NZOs exhibited high blood glucose levels similar to young mice, but no correlation with lower plasma insulin levels was found. Oral glucose application revealed impaired glucose tolerance in all groups, amplified in young mice after the +CH intervention for 14 days. Moreover, glucose intolerance was more pronounced in aged NZO mice before the diet change compared to young counterparts, but no changes due to +CH feeding were observed (Fig. 1D). After the 2-day +CH exposure, elevated plasma insulin levels were observed in young mice, returning to the initial levels after 21 days. In contrast, plasma levels of insulin in aged NZO mice increased continuously during the +CH feeding period and were higher after 21 days compared to young animals (Fig. 1E). In parallel, total pancreatic insulin content decreased in young NZOs in response to the diet change after 21 days, but was unchanged in aged mice. At this timepoint, aged animals fed +CH had 3-fold higher pancreatic insulin content in comparison to their young counterparts (Fig. 1F). By using indirect calorimetry, total values of energy expenditure normalized to body weight were determined, showing comparable results between young and aged NZOs at the end of the +CH intervention (Fig. 1G).

To evaluate functional alterations between beta-cells of young and aged NZO mice, perifusion experiments with freshly isolated islets before and 2 days after the +CH challenge were performed to assess the insulin secretory capacity in response to glucose. Insulin secretion was comparable in islets of young and aged mice before the diet change. After the +CH intervention, young NZO islets show massively elevated first and second phase of insulin release and a delayed adjustment to low glucose conditions. In comparison, islets of aged animals in response to the +CH feeding exhibited also higher insulin secretion under high glucose conditions and responded with gradual decreasing release of insulin when kept on low glucose. No significant difference (p < 0.07) in islet insulin secretion was found comparing aged NZO mice before and after the +CH intervention (Fig. 1H).

3.2. Different impact of the carbohydrate intervention on beta-cell mass in young and aged NZO mice

To assess islet morphology in young and aged mice, immunohistochemical DAB staining against insulin as well as multicolor immunofluorescent labeling of main cell types in pancreatic islets, including beta-cells (insulin), alpha-cells (glucagon), and delta-cells (somatostatin) were performed. In response to the +CH intervention, young NZO mice displayed massive islet rupture and a loss of the characteristic murine islet structure (beta-cells surrounded by alpha-cells), as described earlier [32]. Quantification of beta-cell mass showed a reduction of 42.5% in young +CH challenged NZO mice between day 2 and 21. Interestingly, aged NZOs revealed a marked beta-cell mass

expansion already after 2 days of +CH feeding. At the end of the intervention, beta-cell mass of aged NZOs was more than 2.5-fold higher compared to their young counterparts (Fig. 2A and B). No changes were observed in the islet number, but young NZO mice showed a lower nuclei number per islet after 21 days of the +CH intervention compared to aged animals (Fig. 2C and D). By using TUNEL assay technique, a massive increase in the percentage of TUNEL$^+$-cells within the insulin$^+$-area was found only in young NZO mice in response to the +CH intervention. Notably, the number of apoptotic cells was 2.5-fold higher in young compared to aged NZOs, 21 days after the diet switch (Fig. 2E).

3.3. Transcriptomic profiling identified differences in proliferation, cell cycle and redox related pathways in response to the carbohydrate challenge

To unravel the molecular basis underlying the different islet phenotypes in young compared to aged NZO mice in response to the carbohydrate intervention, a microarray-based transcriptome analysis of isolated pancreatic islets before and after 2 days of the diet change (time point when first functional and morphological differences were observed) was performed. As shown in Fig. 3A, expression of 1.461 transcripts in young and 1.440 transcripts in aged NZO mice were altered after +CH feeding. Among these, a total number of 519 transcripts were dysregulated in both comparisons. By using QIAGEN ingenuity pathway analysis (IPA), ranking of top 10 up- and downregulated transcripts was conducted, indicating differences particularly in transcripts related to proliferation and cell cycle processes. Antigen Ki67 (*Mki67*) was transcriptionally upregulated in both age groups, whereas kinesin family member 4a (*Kif4a*) or centromere protein f (*Cenpf*) expression increased only in aged NZO mice after the carbohydrate challenge. Interestingly, transcripts related to the TXN pathway, such as *Txnip* were upregulated exclusively in islets of young NZOs after the +CH challenge (Fig. 3B, Supplementary Table 1). IPA further revealed an upregulation of cell cycle pathways in young as well as aged NZO mice in response to the +CH intervention. However, the upregulation of some of these pathways, such as cell cycle control of chromosomal replication or estrogen mediated S-phase entry, were more pronounced in aged NZO mice due to +CH feeding (Fig. 3C). Along with this, Gene Ontology (GO) enrichment analysis identified cellular and metabolic processes involved in cell cycle progression that, in turn, were preferentially increased in islets of these mice (Fig. 3D).

3.4. Beta-cell proliferation is more pronounced in islets of aged NZO mice

Since *Mki67* was among the top 5 upregulated transcripts in young and aged NZO mice after +CH exposure, it has been verified whether increased proliferation was associated with beta-cell mass expansion in aged mice. Therefore, RT-PCR analysis in isolated islets and immunohistochemical staining in pancreatic tissue sections were performed. *Mki67* gene expression was massively increased in response to the +CH intervention in both young and aged NZOs, but islets of aged NZO mice revealed 2-fold higher mRNA levels in comparison to their young counterparts (Fig. 4C). Importantly, similar results were found for protein levels. Aged NZO mice had a higher number of Ki67$^+$-nuclei compared with young animals after 2 days of the +CH intervention. This was accompanied by a simultaneous decrease in the number of proliferating cells after 21 days of +CH challenging in young and aged animals (Fig. 4A).

Microarray data revealed no changes in the expression of *Pdx1* between the groups, but mRNA levels determined by RT-PCR were increased by 3-fold in young as well as in aged NZOs in response to the +CH challenge (Supplementary Fig. S1, Fig. 4C). By double immunofluorescent labeling against PDX1 and insulin (to highlight the beta-cell area), no differences were observed comparing aged NZO mice before and 2 days after the +CH intervention. However, young NZO mice after 21 days revealed a decrease by almost 20-30% in the number of PDX1$^+$-
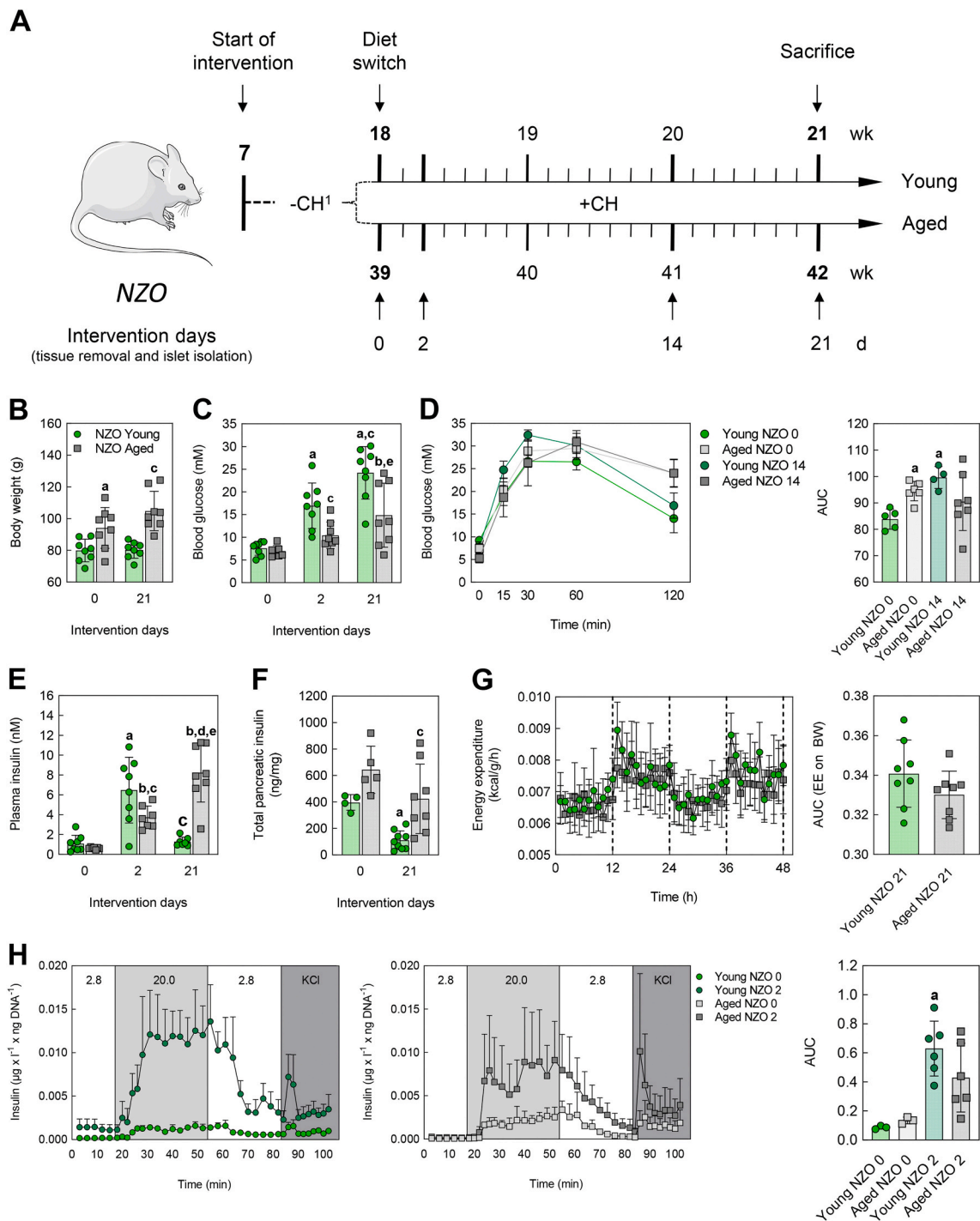
Fig. 1. Glucose utilization and glucose-stimulated insulin secretion of young and aged NZO mice in response to the carbohydrate intervention. (A) Study design and experimental setup. New Zealand obese (NZO) mice received a metabolic challenge composed of carbohydrate-free diet (-CH) for 11 (young) or 32 (aged) weeks[1], followed by carbohydrate-containing diet (+CH) for a maximum of 21 days. **(B)** Body weights (n = 8) and **(C)** blood glucose levels (n = 7–8) of young (green) and aged (grey) NZOs at indicated time points. **(D)** Oral glucose tolerance test with corresponding area under the curve (AUC) of young and aged animals at day 0 and 14 days after the diet change (n = 4–7). **(E)** Plasma insulin levels (n = 7–8) and **(F)** total pancreatic insulin content (n = 4–9) in young and aged NZO mice at indicated time points. **(G)** Energy expenditure (referred to body weight) measured by indirect calorimetry with corresponding AUC of young and aged NZO mice 21 days after + CH feeding (n = 8). **(H)** Glucose-stimulated insulin secretion (perifusion experiment) of freshly isolated pancreatic islets from young and aged NZOs before and after 2 days of the +CH intervention (n = 3–6) with corresponding AUC. Data are represented as mean ± SD. Statistical significance was assessed by Two-tailed Students t-test with Welch correction or two-way ANOVA with Sidak's multiple comparison test, [a,b,c,d,e]$p < 0.05$ (a = significant to young NZO 0, b = significant to aged NZO 0, c = significant to young NZO 2, d = significant to NZO aged 2, e = significant to young NZO 21). (For interpretation of the references to color in this figure legend, the reader is referred to the Web version of this article.)
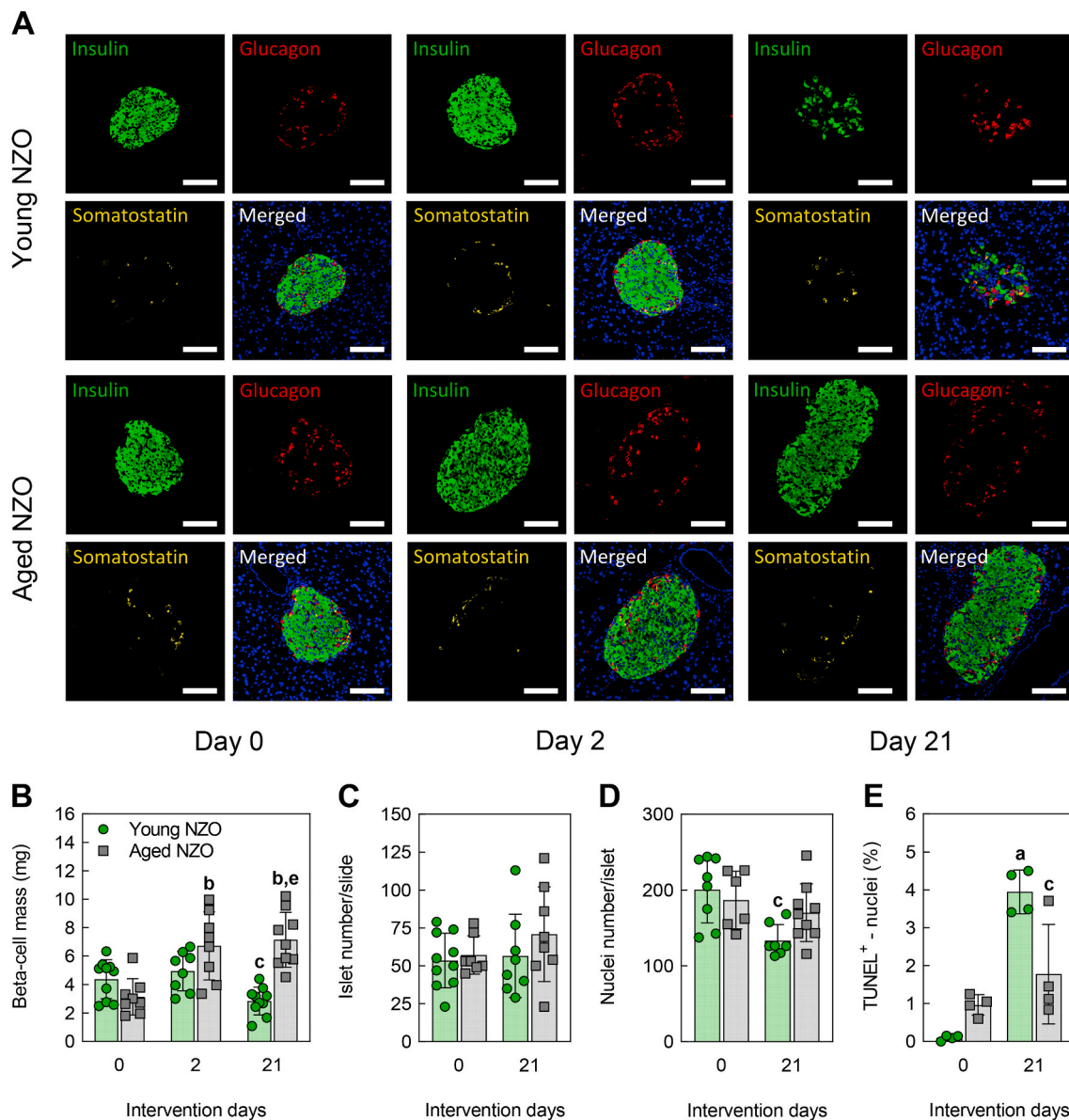
Fig. 2. Morphology and TUNEL-assay of young and aged NZO mice before and after carbohydrate feeding. (A) Representative images (20x magnification) showing multi-color immunofluorescent staining in longitudinal, serial sections from young and aged NZO mice at indicated time points. Green = insulin, red = glucagon, yellow = somatostatin, blue = DAPI. Scale bars, 50 μm. **(B)** Beta-cell mass, **(C)** total islet number per slide and **(D)** total nuclei number per islet in young (green) and aged (grey) NZOs before and 2 as well as 21 days after + CH feeding (n = 8–10). **(E)** Quantification of TUNEL$^+$-nuclei, given as percentage of total nuclei number within the insulin$^+$-area (n = 4). Results are represented as mean values ± SD. Statistical significance was assessed by two-way ANOVA with Sidak's multiple comparison test, $^{a,b,c,e}p < 0.05$ (a = significant to young NZO 0, b = significant to aged NZO 0, c = significant to young NZO 2, e = significant to young NZO 21). (For interpretation of the references to color in this figure legend, the reader is referred to the Web version of this article.)
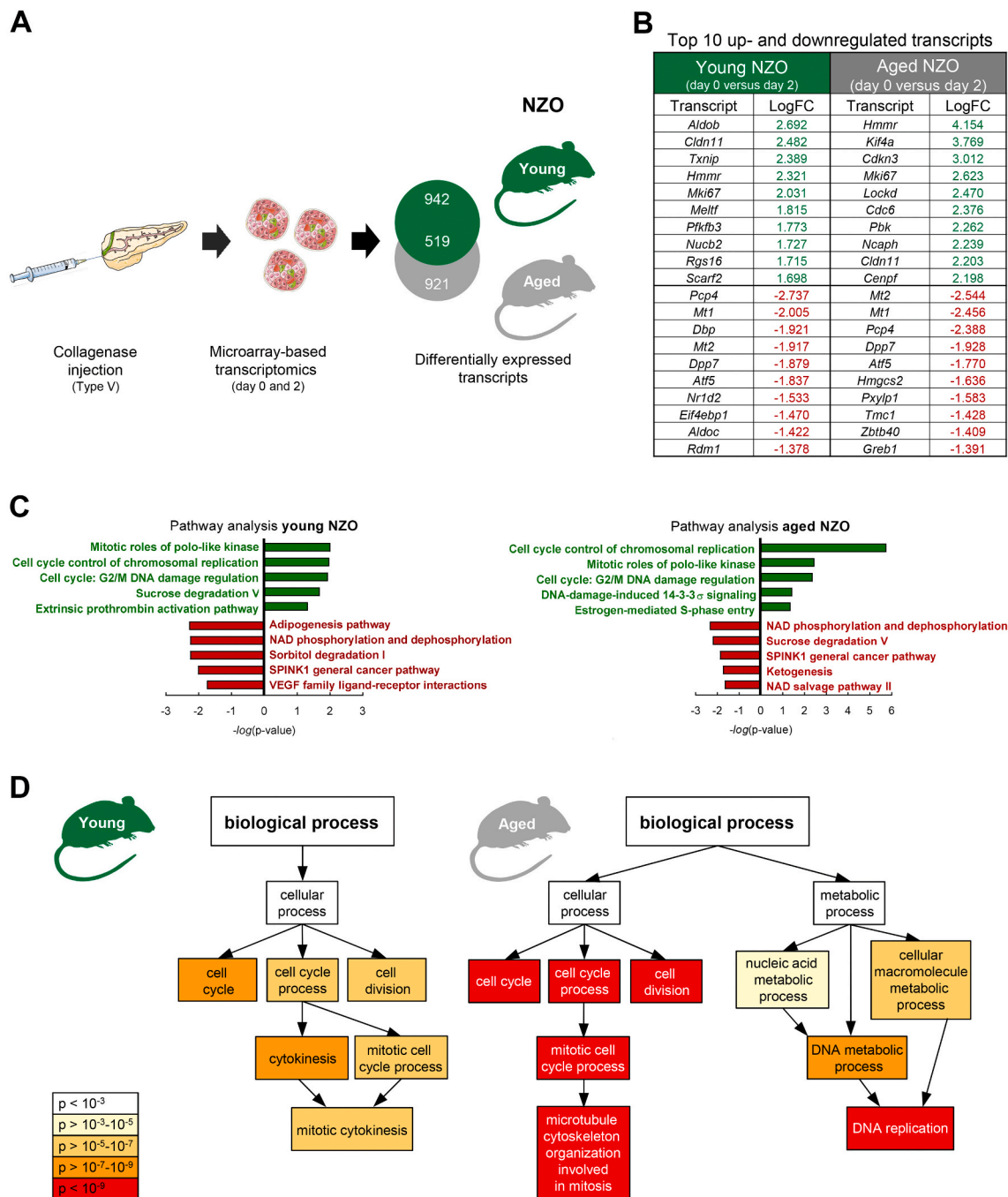
nuclei compared to untreated or aged counterparts (Fig. 4B). Only minor differences were observed in key transcripts for beta-cell identity and maturity after 2 days of the +CH intervention in young and aged NZO islets, as displayed in Supplementary Fig. S1. Expression of neuronal differentiation 1 (*Neurod1*) and urocortin 3 (*Ucn3*), crucial for beta-cell functional maturation, were downregulated in both young and aged NZO mice, whereas the endocrine progenitor marker neurogenin 3 (*Ngn3*) was upregulated exclusively in islets of aged animals. More importantly, IPA identified major differences in transcripts essential for cell cycle progression. Several *Cyclins* and *Cdks* were transcriptionally upregulated, especially in islets of aged NZO mice in response to the +CH intervention, such as *Cyclin A2, E1, B1, B2* and *Cdk1* (Supplementary Fig. S1). RT-PCR analysis further revealed that gene expression levels of almost all determined *Cyclins* and *Cdks* were increased in both age groups after a 2-day +CH exposure, except of *Cyclin D1* and *E1* in

young mice. However, significantly higher mRNA levels of *Cyclin A2, B1, Cdk1, 2* and *4* were found in aged +CH challenged animals compared to their young counterparts (Fig. 4C).

3.5. Beta-cell loss in young NZO mice is associated with increased TXNIP expression and downstream pathways

TXNIP has been shown to be a key regulator in beta-cell apoptosis under hyperglycemic conditions [13,35]. To determine whether TXNIP mediates the loss of beta-cells observed in young mice after +CH feeding, *Txnip* gene and TXNIP protein expression levels as well as components of downstream mechanisms were examined. As mentioned above, IPA identified *Txnip* among the top 3 upregulated transcripts only in young NZO mice after 2 days of the +CH intervention (Fig. 3B). By performing RT-PCR analysis in isolated islets, markedly increased *Txnip*

A

Collagenase injection (Type V)

Microarray-based transcriptomics (day 0 and 2)

Differentially expressed transcripts

NZO

Young

Aged

942
519
921

B

Top 10 up- and downregulated transcripts

Young NZO (day 0 versus day 2)		Aged NZO (day 0 versus day 2)	
Transcript	LogFC	Transcript	LogFC
Aldob	2.692	Hmmr	4.154
Cldn11	2.482	Kif4a	3.769
Txnip	2.389	Cdkn3	3.012
Hmmr	2.321	Mki67	2.623
Mki67	2.031	Lockd	2.470
Meltf	1.815	Cdc6	2.376
Pfkfb3	1.773	Pbk	2.262
Nucb2	1.727	Ncaph	2.239
Rgs16	1.715	Cldn11	2.203
Scarf2	1.698	Cenpf	2.198
Pcp4	-2.737	Mt2	-2.544
Mt1	-2.005	Mt1	-2.456
Dbp	-1.921	Pcp4	-2.388
Mt2	-1.917	Dpp7	-1.928
Dpp7	-1.879	Atf5	-1.770
Atf5	-1.837	Hmgcs2	-1.636
Nr1d2	-1.533	Pxylp1	-1.583
Eif4ebp1	-1.470	Tmc1	-1.428
Aldoc	-1.422	Zbtb40	-1.409
Rdm1	-1.378	Greb1	-1.391

C

Pathway analysis **young NZO**

Mitotic roles of polo-like kinase
Cell cycle control of chromosomal replication
Cell cycle: G2/M DNA damage regulation
Sucrose degradation V
Extrinsic prothrombin activation pathway

Adipogenesis pathway
NAD phosphorylation and dephosphorylation
Sorbitol degradation I
SPINK1 general cancer pathway
VEGF family ligand-receptor interactions

-3 -2 -1 0 1 2 3
-log(p-value)

Pathway analysis **aged NZO**

Cell cycle control of chromosomal replication
Mitotic roles of polo-like kinase
Cell cycle: G2/M DNA damage regulation
DNA-damage-induced 14-3-3σ signaling
Estrogen-mediated S-phase entry

NAD phosphorylation and dephosphorylation
Sucrose degradation V
SPINK1 general cancer pathway
Ketogenesis
NAD salvage pathway II

-3 -2 -1 0 1 2 3 4 5 6
-log(p-value)

D

Young

biological process

cellular process

cell cycle | cell cycle process | cell division

cytokinesis | mitotic cell cycle process

mitotic cytokinesis

p < 10^-3
p > 10^-3-10^-5
p > 10^-5-10^-7
p > 10^-7-10^-9
p < 10^-9

Aged

biological process

cellular process | metabolic process

cell cycle | cell cycle process | cell division

nucleic acid metabolic process | cellular macromolecule metabolic process

mitotic cell cycle process

DNA metabolic process

microtubule cytoskeleton organization involved in mitosis

DNA replication

Fig. 3. Microarray-based transcriptomics in young and aged NZO islets before and 2 days after the carbohydrate intervention. **(A)** Simplified experimental setup of islet isolation and total numbers of differentially expressed transcripts obtained from microarray in young (green) and aged (grey) NZO islets before and 2 days after the +CH intervention (n = 5). **(B)** Top 10 list of differentially regulated transcripts and **(C)** ingenuity pathway analysis (IPA), showing top 5 up- (green) and downregulated (red) pathways at day 0 and 2 days after the diet change. **(D)** Classified visualization of mainly enriched Gene Ontology (GO) terms by upregulated transcripts. P-values for enrichments were p < 10^-6 in young or p < 10^-11 in aged NZO mice, respectively. (For interpretation of the references to color in this figure legend, the reader is referred to the Web version of this article.)

mRNA levels were found in both young and aged NZO mice in response to +CH feeding. However, direct comparison of the groups fed +CH revealed higher mRNA expression of *Txnip* by 55% in young animals (Fig. 5A). Immunoblotting of islet lysates confirmed such changes, showing an increase in TXNIP protein expression after a 2-day +CH intervention only in young NZO mice, returning to the initial level after 21 days. Protein levels of TXNIP were unchanged in aged NZO mice and lower compared to young animals after 2 and 21 days of +CH feeding (Fig. 5B).

Although microarray data revealed an upregulation of *Txn1*

expression only in young NZOs fed +CH, mRNA levels determined by RT-PCR were increased in both young and aged NZO islets in response to the +CH intervention with no difference between the groups. Transcriptional *Txn2* expression was unchanged in both age groups, but islets from young NZOs on a +CH diet showed lower *Txn2* mRNA levels compared to the untreated ones. In contrast, gene expression levels of *Txn2* where lower in aged compared to young mice before the diet switch and unchanged in response to +CH exposure (Supplementary Fig. S1, Fig. 5A). As shown in previous investigations, downregulation of *Txn2* gene expression is associated with an induction of the apoptotic
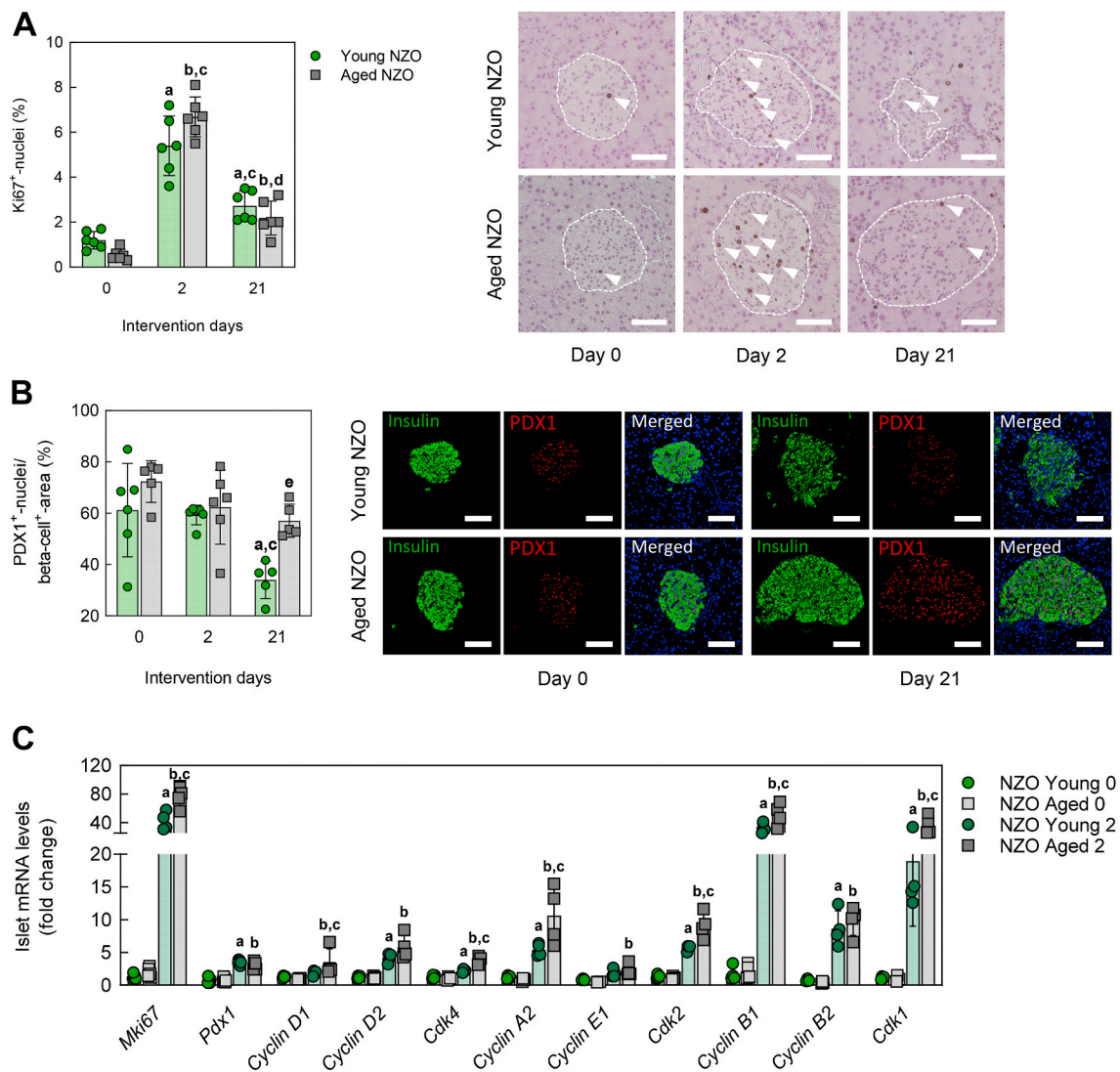
Fig. 4. Proliferation and cell cycle analysis in young and aged NZO mice before and after the carbohydrate challenge. (A, B) Quantification of immunostainings against Ki67 (n = 6) and PDX1 (co-stained with insulin, n = 5–6), given as percentage of positive stained nuclei per islet or insulin$^+$-area, respectively and representative images (20x magnification) of pancreatic sections of young and aged NZOs at indicated time points. White lines and arrows mark the islet area and Ki67$^+$-nuclei, respectively. Green = insulin, red = PDX1, blue = DAPI. Scale bars, 50 μm. **(C)** RT-PCR analysis of cell cycle-related genes in isolated islets from young and aged NZO mice at day 0 and day 2 after +CH feeding (n = 4–6). Data are represented as mean ± SD. Statistical significance was assessed by two-way ANOVA with Sidak's multiple comparison test, ^{a,b,c,d,e}p < 0.05 (a = significant to young NZO 0, b = significant to aged NZO 0, c = significant to young NZO 2, d = significant to aged NZO 2, e = significant to young NZO 21). (For interpretation of the references to color in this figure legend, the reader is referred to the Web version of this article.)

signaling pathway via increased phosphorylation of apoptosis signal-regulating kinase 1 (ASK1) and activation of caspase-3 [36]. Thus, caspase-3 was examined by immunostaining, indicating elevated numbers of caspase-3$^+$-nuclei, in young +CH challenged NZO mice after 21 days that was also observed when compared to their aged counterparts (Fig. 5C).

4. Discussion

In the present study, we investigated the impact of aging on beta-cell functionality and integrity under diet-induced metabolic stress in diabetes-prone NZO mice. The important finding of our work was that aged mice compensated metabolic stress due to beta-cell mass expansion, whereas young NZOs exhibited massive beta-cell damage, generating a diabetes-like phenotype. Particularly by comparing gene, but also protein expression profiles, we found that proliferation via cell cycle activation was more pronounced and redox balance was preserved in

islets of aged animals. With this, our data provide insights into molecular changes in beta-cell functionality and structural integrity in advanced age under metabolic stress conditions.

Type 2 diabetes development occurs typically in response to overnutrition and physical inactivity, contributing to insulin resistance, obesity and metabolic stress [37,38]. By increased secretion and beta-cell mass expansion, islets are able to adjust on elevated insulin requirements. However, sustained stress conditions decrease the islet compensatory capacity in most obese individuals, leading to a loss of functional beta-cells and the onset and progression of type 2 diabetes with increasing age [39–41]. Mouse models prone to postprandial metabolic stress, such as NZO mice, mimic the human obesity-associated type 2 diabetes and were used in the present study. As previously described, young NZO mice exhibited obesity and insulin resistance when kept on a diet without carbohydrates, followed by depletion of insulin stores and a progressive loss of functional beta-cells in response to a carbohydrate intervention [27,31,32,34,42]. These mice showed
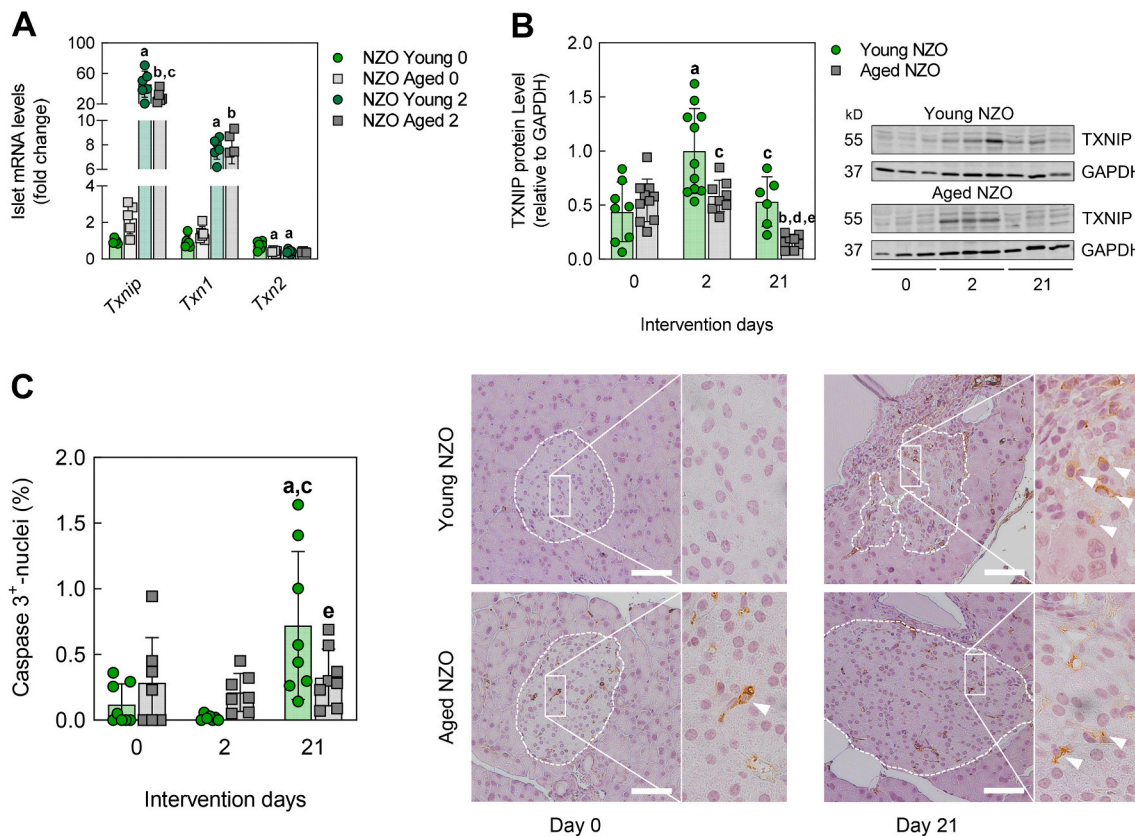
Fig. 5. Thioredoxin-interacting protein expression and downstream mechanisms in young and aged NZO mice in response to carbohydrate feeding. (A) RT-PCR analysis of thioredoxin (TXN) pathway-related genes (n = 5–6) and **(B)** immunoblot analysis of thioredoxin-interacting protein (TXNIP) with representative blots (n = 6–11) in islets isolated from young (green) and aged (grey) NZOs at indicated time points. **(C)** Morphometric analysis of caspase-3 immunostaining, determined as percentage of positive stained nuclei per islet of young and aged NZO mice before and 2 as well as 21 days after the +CH intervention with representative images (20x and 60x magnification) in pancreatic tissue sections (n = 6–8). White lines and arrows mark the islet area or caspase-3⁺-nuclei, respectively. Scale bars, 50 μm. Results are presented as mean values ± SD. Statistical significance was assessed by two-way ANOVA with Sidak's multiple comparison test, $^{a,b,c,d,e}p < 0.05$ (a = significant to young NZO 0, b = significant to aged NZO 0, c = significant to young NZO 2, d = significant to aged NZO 2, e = significant to young NZO 21). (For interpretation of the references to color in this figure legend, the reader is referred to the Web version of this article.)

distinct body weight gain due to *ad libitum* availability to the high-caloric carbohydrate-free diet. The carbohydrate intervention rapidly induced hyperglycemia, accompanied by islet secretory dysfunction, as indicated by abnormal insulin release and the inability to adjust on changing glucose concentrations. A subsequent decrease in pancreatic insulin content and circulating insulin levels, combined with reduced PDX1 protein expression, point out a poor glycemic control and suggest islet functional exhaustion in young NZO mice. In parallel, massive islet rupture with pancreatic beta-cells loss by apoptosis was induced, presumably initiating a vicious cycle of continuously increasing glucose levels, beta-cell damage and reduced insulin production. Although prolonged feeding without carbohydrates leads to further body weight gain and impairment of glucose tolerance, aged mice exhibited only moderate hyperglycemia by progressively increasing plasma and unchanged pancreatic insulin levels in response to the carbohydrate intervention. This was mediated by preserved beta-cell functionality as well as fast and marked beta-cell mass expansion. Similar findings were shown in a recent study by De Leon et al. using male C57BL/6J mice aged 22 months. Although young as well as aged mice exhibited a distinct increase in beta-cell mass following a western-diet administration for 4 weeks, *ex vivo* insulin secretion was only maintained in older animals [43].

RNA profiling analysis discovered several cell cycle and proliferation-related genes that were upregulated in response to the carbohydrate intervention in islets of young as well as aged mice. However, gene expression levels of Ki67, *Cyclin D1* and *Cdk4* were

higher in aged compared to young mice after carbohydrate feeding. The particular role of the so-called "early" cyclins and CDKs, precisely controlling G1/S-phase transition in beta-cell proliferation and mass expansion in murine islets, has been shown in a high number of excellent publications, using genetically modified mouse models [44–48]. Alonso et al. further revealed a dose- and time-dependent increase in *Cyclin D2* gene and protein expression levels after a 4-day glucose infusion, similar to our data [49]. Previous investigations also highlight the importance of "late" cyclins and Cdks (*Cyclin A, E* and *Cdk1, 2*) in cell cycle progression and beta-cell proliferation, but an increased expression of these cell cycle regulatory genes in response to glucose has not been examined so far [50,51]. Here, we found elevated *Cyclin A2* and *Cdk2* mRNA levels in both young and aged NZO mice after carbohydrate exposure with higher levels in aged animals, accompanied by an upregulation of *Cyclin E1* expression. Markedly enhanced levels of mitotic *Cyclin B1* and its complexing partner *Cdk1* were also observed in islets of aged compared to young mice following carbohydrate feeding. To our knowledge, the extent to which this complex is crucial for beta-cell cycle regulation and proliferation has not been elucidated. It was only demonstrated by Ackermann et al. that *Cyclin B1* expression was elevated during islet expansion in a mouse model of partial pancreatectomy [52]. Nevertheless, B-cyclins together with CDK1 are involved in the completion of the cell cycle, indicating their important role within the cell cycle machinery. In combination, upregulation of early, late and mitotic *Cyclins* and *Cdks* accompanied by increased Ki67 expression indicate clearly that beta-cell proliferation is the primary stimulus for beta-cell mass

expansion in aged NZO mice in response to metabolic stress.

In line with an oligonucleotide microarray analysis of islets from human donors by Shalev et al. in 2002, islet transcriptomics further showed that *Txnip*, a scaffold protein triggering beta-cell apoptosis under hyperglycemic conditions, was among the top upregulated transcripts after carbohydrate feeding, exclusively in young NZO islets [13–15,17,53]. The microarray data were confirmed by RT-PCR and immunoblot analysis, consistently demonstrating markedly higher *Txnip* gene and TXNIP protein levels in islets of young NZO mice in response to the carbohydrate intervention compared to their aged counterparts, indicating an induction of redox imbalance. The effects of TXNIP are mediated by several downstream mechanisms dependent on its localization [54]. Cytosolic TXNIP binds and inhibits TXN1, thus, regulating cellular redox state by decreasing the anti-oxidative capacity of the TXN system [55–57]. In contrast to previous studies, we found elevated *Txn1* gene expression in both islets of young and aged NZOs that might be explained by a compensatory mechanism to maintain redox balance of islet cells [57]. With this, we cannot assume that beta-cell apoptosis in young mice was mediated by TXNIP-induced inhibition of TXN1. However, TXNIP has been shown to interfere with TXN2 after shuttling into the mitochondria, where it might trigger an apoptotic signaling cascade via caspase-3 activation [13,36,58]. Notably, only islets of young NZO mice exhibited decreased *Txn2* mRNA expression in response to the carbohydrate challenge. As previously described, this might lead to increased phosphorylation and activation of ASK1, followed by caspase-3 cleavage and finally beta-cell apoptosis [36,59]. A similar observation was made in our study, showing elevated amounts of caspase-3$^+$-nuclei exclusively in pancreatic islets of young carbohydrate challenged NZO mice, consistent with an earlier investigation [32]. Thus, reduced *Txn2* gene expression in combination with elevated capase-3 protein levels suggest a TXNIP-related induction of mitochondrial apoptotic cascade that might initiate beta-cell destruction in young NZO mice under metabolic stress conditions.

TXNIP has been also considered as a tumor suppressor protein, able to inhibit cell proliferation by blocking cell cycle progression. TXNIP stabilizes cell cycle inhibitor proteins, such as p27^{Kip1} and represses *Cyclin A2*, *E* as well as *Cdk2*, consequently preventing G1/S-phase transition and regulating the cell cycle machinery [60–62].

It might be therefore hypothesized that increasing TXNIP expression levels in young carbohydrate-fed NZO mice are also associated with lower levels of cell cycle regulatory genes, thereby preventing an adaptive response towards hyperglycemia. In contrast, an unchanged and apparently balanced TXNIP expression, indicating also sustained redox homeostasis, does not compromise cell cycle activation, thus, presumably contributing to the increase in beta-cell mass observed in aged mice after the carbohydrate intervention. This assumption is strengthened by findings of Chen et al. showing that beta-cell specific *Txnip* deletion in obese, diabetic mice is associated with reduced beta-cell apoptosis and enhanced beta-cell mass expansion [63].

In conclusion, metabolically stressed, young NZO mice developed hyperglycemia in response to a carbohydrate intervention accompanied by insulin hypersecretion, depletion of insulin stores and beta-cell death. This seems to be mediated by increased TXNIP expression, associated with the induction of an apoptotic signaling cascade via caspase-3. Despite elevated metabolic stress, aged NZO mice exhibited only moderate hyperglycemia after carbohydrate exposure due to maintained anti-oxidative potential and increased proliferative capacity by cell cycle activation, thus, ensuring beta-cell mass expansion and islet functionality. However, it is unclear whether aged mice are entirely protected against the loss of functional beta-cell mass that might occur theoretically after further extension of the carbohydrate feeding period. Nevertheless, these findings support the relevance of an unrestricted proliferative potential, presumably associated with redox homeostasis for islet function under metabolic stress conditions, able to prevent beta-cell failure even at advanced age.

Author contributions

Conceptualization, R.K., A.S., T.G. and A.H.; Methodology, R.K., M. J., S.D., T.F., J.K., T.J., M.S. and W.J.; Software, T.J.; Formal Analysis M. J.; Investigation R.K., M.J., S.D., T.F., J.K., T.J., M.S. and W.J.; Writing – Original Draft, R.K. and A.H.; Writing – Review & Editing, All authors; Visualization R.K., M.S. and W.J.; Supervision, A.S., T.G. and A.H.; Project Administration, R.K., T.G. and A.H.; Funding Acquisition, T.G and A.H.

Declaration of interest

The authors declare no competing interest.

Acknowledgements

Appendix A. Supplementary data

Supplementary data to this article can be found online at https://doi.org/10.1016/j.redox.2020.101748.

References

[1] M. Wortham, M. Sander, Mechanisms of beta-cell functional adaptation to changes in workload, Diabetes Obes. Metabol. 18 (Suppl 1) (2016) 78–86.

[2] P.E. MacDonald, J.W. Joseph, P. Rorsman, Glucose-sensing mechanisms in pancreatic beta-cells, Philos. Trans. R. Soc. Lond. B Biol. Sci. 360 (1464) (2005) 2211–2225.

[3] Y. Saisho, et al., beta-cell mass and turnover in humans: effects of obesity and aging, Diabetes Care 36 (1) (2013) 111–117.

[4] A.K. Linnemann, M. Baan, D.B. Davis, Pancreatic beta-cell proliferation in obesity, Adv Nutr 5 (3) (2014) 278–288.

[5] E. Bernal-Mizrachi, et al., Human beta-cell proliferation and intracellular signaling part 2: still driving in the dark without a road map, Diabetes 63 (3) (2014) 819–831.

[6] P. Acosta-Montano, V. Garcia-Gonzalez, Effects of dietary fatty acids in pancreatic beta cell metabolism, implications in homeostasis, Nutrients 10 (4) (2018).

[7] M.F. Brereton, et al., Hyperglycaemia induces metabolic dysfunction and glycogen accumulation in pancreatic beta-cells, Nat. Commun. 7 (2016) 13496.

[8] H.I. Marrif, S.I. Al-Sunousi, Pancreatic beta cell mass death, Front. Pharmacol. 7 (2016) 83.

[9] N. Kaiser, G. Leibowitz, R. Nesher, Glucotoxicity and beta-cell failure in type 2 diabetes mellitus, J. Pediatr. Endocrinol. Metab. 16 (1) (2003) 5–22.

[10] S. Lenzen, J. Drinkgern, M. Tiedge, Low antioxidant enzyme gene expression in pancreatic islets compared with various other mouse tissues, Free Radic. Biol. Med. 20 (3) (1996) 463–466.

[11] N. Hou, et al., Reactive oxygen species-mediated pancreatic beta-cell death is regulated by interactions between stress-activated protein kinases, p38 and c-Jun N-terminal kinase, and mitogen-activated protein kinase phosphatases, Endocrinology 149 (4) (2008) 1654–1665.

[12] A. Sarre, et al., Reactive oxygen species are produced at low glucose and contribute to the activation of AMPK in insulin-secreting cells, Free Radic. Biol. Med. 52 (1) (2012) 142–150.

[13] J. Chen, et al., Thioredoxin-interacting protein: a critical link between glucose toxicity and beta-cell apoptosis, Diabetes 57 (4) (2008) 938–944.

[14] A. Nishiyama, et al., Redox regulation by thioredoxin and thioredoxin-binding proteins, IUBMB Life 52 (1–2) (2001) 29–33.

[15] E. Junn, et al., Vitamin D3 up-regulated protein 1 mediates oxidative stress via suppressing the thioredoxin function, J. Immunol. 164 (12) (2000) 6287–6295.

[16] G. Xu, et al., Thioredoxin-interacting protein regulates insulin transcription through microRNA-204, Nat. Med. 19 (9) (2013) 1141–1146.

[17] P.C. Schulze, et al., Hyperglycemia promotes oxidative stress through inhibition of thioredoxin function by thioredoxin-interacting protein, J. Biol. Chem. 279 (29) (2004) 30369–30374.

[18] E. Yoshihara, et al., Thioredoxin/Txnip: redoxisome, as a redox switch for the pathogenesis of diseases, Front. Immunol. 4 (2014) 514.

[19] R. Kehm, et al., Age-related oxidative changes in pancreatic islets are predominantly located in the vascular system, Redox Biol 15 (2018) 387–393.

[20] V. De Tata, Age-related impairment of pancreatic Beta-cell function: pathophysiological and cellular mechanisms, Front. Endocrinol. 5 (2014) 138.

[21] J.A. Kushner, The role of aging upon beta cell turnover, J. Clin. Invest. 123 (3) (2013) 990–995.

[22] C. Lopez-Otin, et al., The hallmarks of aging, Cell 153 (6) (2013) 1194–1217.

[23] R. Kehm, et al., Endogenous advanced glycation end products in pancreatic islets after short-term carbohydrate intervention in obese, diabetes-prone mice, Nutr. Diabetes 9 (1) (2019) 9.

[24] James G. Fox, F.W. Quimby, Christian E. Newcomer, Muriel T. Davisson, Stephen W. Barthold, Abigail L. Smith, The Mouse in Biomedical Research - History, Wild Mice, and Genetics, 2007, p. 2192.

[25] W.H. Cheng, V.A. Bohr, R. de Cabo, Nutrition and aging, Mech. Ageing Dev. 131 (4) (2010) 223–224.

[26] G. Li, et al., Early postnatal overnutrition accelerates aging-associated epigenetic drift in pancreatic islets, Environ Epigenet 5 (3) (2019) dvz015.

[27] O. Kluth, et al., Identification of four mouse diabetes candidate genes altering beta-cell proliferation, PLoS Genet. 11 (9) (2015), e1005506.

[28] R Development Core Team, R: A Language and Environment for Statistical Computing, R Foundation for Statistical Computing, 2018.

[29] E. Eden, et al., GOrilla: a tool for discovery and visualization of enriched GO terms in ranked gene lists, BMC Bioinf. 10 (2009) 48.

[30] T. Grune, et al., Cyt/nuc," a customizable and documenting ImageJ macro for evaluation of protein distributions between cytosol and nucleus, Biotechnol. J. 13 (5) (2018), e1700652.

[31] H.S. Jurgens, et al., Development of diabetes in obese, insulin-resistant mice: essential role of dietary carbohydrate in beta cell destruction, Diabetologia 50 (7) (2007) 1481–1489.

[32] O. Kluth, et al., Dissociation of lipotoxicity and glucotoxicity in a mouse model of obesity associated diabetes: role of forkhead box O1 (FOXO1) in glucose-induced beta cell failure, Diabetologia 54 (3) (2011) 605–616.

[33] F. Mirhashemi, et al., Diet dependence of diabetes in the New Zealand Obese (NZO) mouse: total fat, but not fat quality or sucrose accelerates and aggravates diabetes, Exp. Clin. Endocrinol. Diabetes 119 (3) (2011) 167–171.

[34] O. Kluth, et al., Decreased expression of cilia genes in pancreatic islets as a risk factor for type 2 diabetes in mice and humans, Cell Rep. 26 (11) (2019) 3027–3036 e3.

[35] A. Shalev, Lack of TXNIP protects beta-cells against glucotoxicity, Biochem. Soc. Trans. 36 (Pt 5) (2008) 963–965.

[36] G. Saxena, J. Chen, A. Shalev, Intracellular shuttling and mitochondrial function of thioredoxin-interacting protein, J. Biol. Chem. 285 (6) (2010) 3997–4005.

[37] S. Cernea, M. Dobreanu, Diabetes and beta cell function: from mechanisms to evaluation and clinical implications, Biochem. Med. 23 (3) (2013) 266–280.

[38] S.Z. Hasnain, J.B. Prins, M.A. McGuckin, Oxidative and endoplasmic reticulum stress in beta-cell dysfunction in diabetes, J. Mol. Endocrinol. 56 (2) (2016) R33–R54.

[39] V.S. Moulle, J. Ghislain, V. Poitout, Nutrient regulation of pancreatic beta-cell proliferation, Biochimie 143 (2017) 10–17.

[40] M. Cnop, et al., Mechanisms of pancreatic beta-cell death in type 1 and type 2 diabetes: many differences, few similarities, Diabetes 54 (Suppl 2) (2005) S97–S107.

[41] G.C. Weir, S. Bonner-Weir, Islet beta cell mass in diabetes and how it relates to function, birth, and death, Ann. N. Y. Acad. Sci. 1281 (2013) 92–105.

[42] O. Kluth, et al., Differential transcriptome analysis of diabetes-resistant and -sensitive mouse islets reveals significant overlap with human diabetes susceptibility genes, Diabetes 63 (12) (2014) 4230–4238.

[43] E.R. De Leon, et al., Age-dependent protection of insulin secretion in diet induced obese mice, Sci. Rep. 8 (1) (2018) 17814.

[44] J.A. Kushner, et al., Cyclins D2 and D1 are essential for postnatal pancreatic beta-cell growth, Mol. Cell Biol. 25 (9) (2005) 3752–3762.

[45] S. Georgia, A. Bhushan, Beta cell replication is the primary mechanism for maintaining postnatal beta cell mass, J. Clin. Invest. 114 (7) (2004) 963–968.

[46] S.I. Tschen, et al., Cyclin D2 is sufficient to drive beta cell self-renewal and regeneration, Cell Cycle 16 (22) (2017) 2183–2191.

[47] S.G. Rane, et al., Loss of Cdk4 expression causes insulin-deficient diabetes and Cdk4 activation results in beta-islet cell hyperplasia, Nat. Genet. 22 (1) (1999) 44–52.

[48] X. Zhang, et al., Overexpression of cyclin D1 in pancreatic beta-cells in vivo results in islet hyperplasia without hypoglycemia, Diabetes 54 (3) (2005) 712–719.

[49] L.C. Alonso, et al., Glucose infusion in mice: a new model to induce beta-cell replication, Diabetes 56 (7) (2007) 1792–1801.

[50] W.J. Song, et al., Exendin-4 stimulation of cyclin A2 in beta-cell proliferation, Diabetes 57 (9) (2008) 2371–2381.

[51] S. Tiwari, et al., Early and late G1/S cyclins and Cdks act complementarily to enhance authentic human beta-cell proliferation and expansion, Diabetes 64 (10) (2015) 3485–3498.

[52] A. Ackermann Misfeldt, R.H. Costa, M. Gannon, Beta-cell proliferation, but not neogenesis, following 60% partial pancreatectomy is impaired in the absence of FoxM1, Diabetes 57 (11) (2008) 3069–3077.

[53] A. Shalev, et al., Oligonucleotide microarray analysis of intact human pancreatic islets: identification of glucose-responsive genes and a highly regulated TGFbeta signaling pathway, Endocrinology 143 (9) (2002) 3695–3698.

[54] A. Shalev, Minireview: thioredoxin-interacting protein: regulation and function in the pancreatic beta-cell, Mol. Endocrinol. 28 (8) (2014) 1211–1220.

[55] H. Yamanaka, et al., A possible interaction of thioredoxin with VDUP1 in HeLa cells detected in a yeast two-hybrid system, Biochem. Biophys. Res. Commun. 271 (3) (2000) 796–800.

[56] P. Patwari, et al., The interaction of thioredoxin with Txnip. Evidence for formation of a mixed disulfide by disulfide exchange, J. Biol. Chem. 281 (31) (2006) 21884–21891.

[57] A. Nishiyama, et al., Identification of thioredoxin-binding protein-2/vitamin D(3) up-regulated protein 1 as a negative regulator of thioredoxin function and expression, J. Biol. Chem. 274 (31) (1999) 21645–21650.

[58] J. Chen, et al., Lack of TXNIP protects against mitochondria-mediated apoptosis but not against fatty acid-induced ER stress-mediated beta-cell death, Diabetes 59 (2) (2010) 440–447.

[59] M. Saitoh, et al., Mammalian thioredoxin is a direct inhibitor of apoptosis signal-regulating kinase (ASK) 1, EMBO J. 17 (9) (1998) 2596–2606.

[60] S.H. Han, et al., VDUP1 upregulated by TGF-beta1 and 1,25-dihydorxyvitamin D3 inhibits tumor cell growth by blocking cell-cycle progression, Oncogene 22 (26) (2003) 4035–4046.

[61] M.G. Elgort, et al., Transcriptional and translational downregulation of thioredoxin interacting protein is required for metabolic reprogramming during G(1), Genes Cancer 1 (9) (2010) 893–907.

[62] K. Kamitori, et al., Both Ser361 phosphorylation and the C-arrestin domain of thioredoxin interacting protein are important for cell cycle blockade at the G1/S checkpoint, FEBS Open Bio 8 (11) (2018) 1804–1819.

[63] J. Chen, et al., Thioredoxin-interacting protein deficiency induces Akt/Bcl-xL signaling and pancreatic beta-cell mass and protects against diabetes, Faseb. J. 22 (10) (2008) 3581–3594.